Jet Energy Scale and Quark Compositeness with ATLAS

Frank Berghaus

Committee:

Michel Lefebvre, Stan Dosso, Robert McPherson, Randy Sobie

April 24, 2008

Abstract

ATLAS will explore the possibility that the fundamental particles of the Standard Model of particle physics are composite. With the first fb^{-1} of physics data ATLAS will be able to probe compositeness to 14 TeV (10^{-20} m). The unexplored energies of the collisions produced by the LHC for ATLAS yield a complex environment to investigate for new physics. Data driven approaches using top pair production to assess the calibration of hadronic jets will be developed. The inclusive jet cross-section, two-jet angular spectrum and two-jet mass spectrum are explored as avenues to probe for structure within quarks. The importance of jet calibration for the compositeness measurement is discussed in each case.

Contents

1 Introduction

The Large Hadron Collider (LHC) will allow the exploration of many new physics ideas beyond the Standard Model. One exciting possibility is that the fundamental particles of the Standard Model are composite. Compositeness could explain the wealth of particles (61 or 58) in the Standard Model, and explain it's structure. Exploring compositeness requires a good understanding of jets observed from the collisions soon to be produced at the LHC. This section will introduce the experimental environment of the LHC. Chapter 2 will discuss how to calibrate the energy of jets from data. Chapter 3 will explore different ways compositeness could be measured and the uncertainties of the measurement.

1.1 ATLAS And The LHC

The LHC is now constructed and entering it's commissioning phase at the European Organization for Nuclear Research (CERN). The LHC is planned to deliver it's first beam of 900 GeV momentum[1] protons in May 2008 and to accelerate two counter-rotating proton beams to 7 TeV in September 2008. The proton beams can collide at four interaction points as displayed in figure 1. A Toroidal LHC ApparatuS (ATLAS) and the Compact Muon Spectrometer (CMS) are the two multi-purpose detectors that will investigate the 14 TeV pp collisions for signs of new physics beyond our current knowledge.

The collisions observed by ATLAS will be of protons. Protons are composite particles containing three valence quarks (two up-quarks and one down-quark). Most of the protons mass is in fact carried in the binding energy of the valence quarks. The proton contains seaquarks and gluons. All these constituents are referred to as partons. Each parton carries some fraction of the protons momentum. The distribution of the proton's momentum among it's constituents is described by parton distribution functions (PDFs). The CTEQ [1] and MRS [2] groups fit their models of the PDFs to existing data from deep inelastic scattering in lepton-lepton, lepton-hadron and hadron-hadron collisions.

Since the momentum of the proton is distributed among it's constituents as displayed in figure 2,

[1]Natural units for particle physics set $c = \hbar = 1$ and express energy, momentum and mass in units of eV.

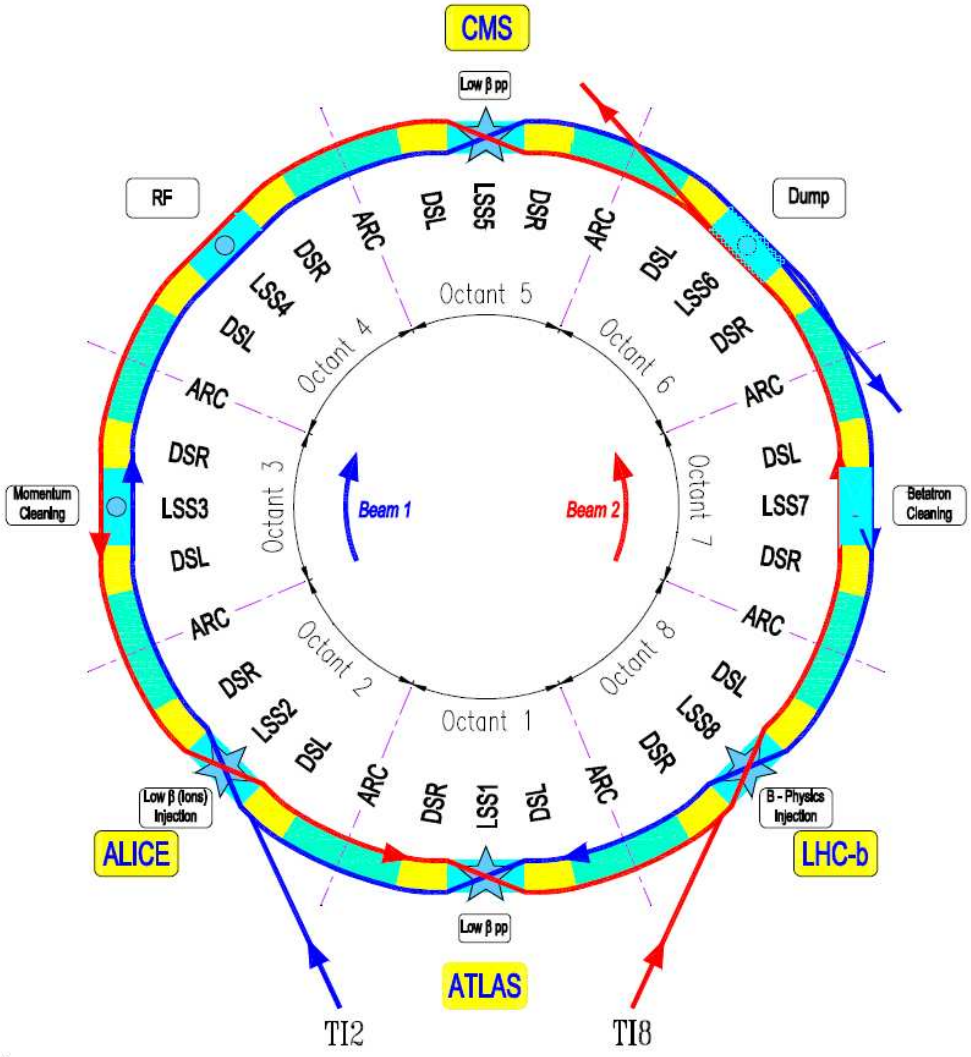

Figure 1: Schematic of the LHC. The are long straight sections (LSS) contain the accelerating parts. The dispersion suppressors (DS) ensure that the proton beams stay focused.

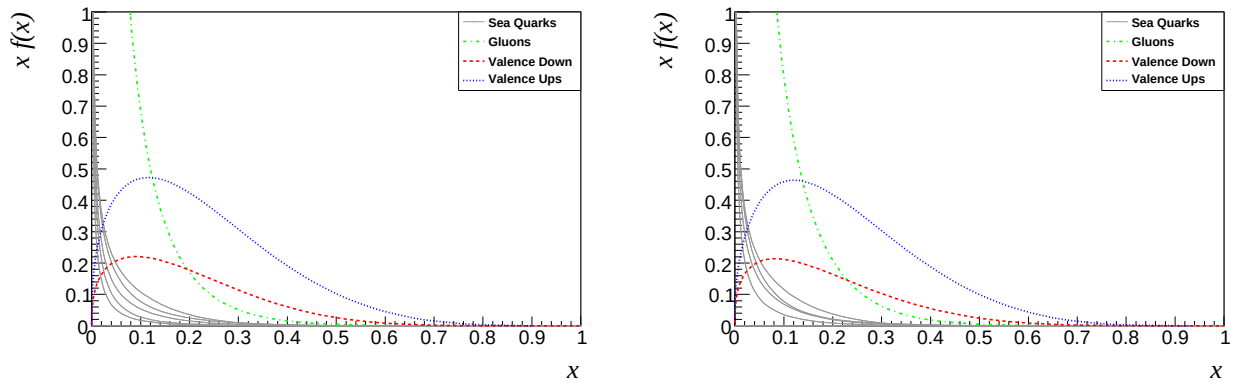

(a) (b)

Figure 2: The (a) CTEQ and (b) MRST leading order fits of the proton's parton distribution functions at 400 GeV of momentum transfer [3].

we do not know a priory the longitudinal velocity of the centre of momentum of each collision. Conservation of momentum can only be applied in the plane transverse to the beam because the partons start with no or very little momentum transverse to the beam axis.

For hard scatter events only two partons interact in the collision of the protons. The rest of the protons' constituents give rise to the *underlying event*. It reflects the fact that all the partons of the proton are tied together though the strong force. The underlying event is connected to the hard scatter of interest and varies with each physics process.

The LHC will initially supply a luminosity of up to $\mathcal{L} = 10^{31}$ cm^{-2}s^{-1}. After a few months of running the luminosity will be increased to 10^{33} cm^{-2}s^{-1}. The protons in each beam will be delivered in bunches that cross in the ATLAS detector every 75 ns. Later the luminosity will be increased even further by changing the time between bunch crossings to 25 ns. Initially one or less interaction per bunch crossing is expected. At full luminosity around 22 interactions per bunch crossing are expected. The typical detector response time for ATLAS is about 20 to 50 ns. At full luminosity (25 ns time between bunch crossings) ATLAS will be sensitive to 20 to 50 low $p_\perp$ scatter events (largest cross-section) along with any interesting physics events that triggered the event readout. These background events are called *pile-up*.

The ATLAS detector has symmetries in the azimuthal angle ϕ. ϕ is invariant under boosts along the beamline. Longitudinal to the beam the detector is segmented in pseudorapidity (ex-

plained in section 1.2). The pseudorapidity gives the polar angle. Differences in pseudorapidity are invariant under boosts along the beamline. Therefore differential cross-sections in pseudorapidity are invariant under longitudinal boosts, so every interval of pseudorapidity should see the same amount of noise from pile-up events. This is referred to as *pile-up noise*.

Because of the wealth of information that needs to be read out for each event from the ATLAS detector, it will only be possible to write about 100 events to disk per second. This means the expected 13 MHz rate of events must be reduced. This is achieved by three levels of trigger algorithms monitoring the data for interesting events. The least biased events are required to leave hits in both the forward and backward regions of the detector[2]. All events that pass this trigger are referred to as *minimum bias* events. At full luminosity 22 minimum bias events are expected from each bunch crossing.

1.2 Coordinate System

The ATLAS coordinate system is right handed and centred on the detector[3]. The z-axis runs along the beam. The y-axis points up and the x-axis points towards the centre of the LHC ring. A Cartesian system is cumbersome to express the 4-momenta of particles measured with ATLAS, so another system is defined as:

$$\begin{aligned} p &= (E, p_x, p_y, p_z) \\ &= (m_\perp \cosh\eta, p_\perp \cos\phi, p_\perp \sin\phi, m_\perp \sinh\eta) \end{aligned} \tag{1}$$

where ϕ is the azimuthal angle measured from the x-axis, $p_\perp$ is the transverse component of the 3-momentum $\sqrt{p_x^2 + p_y^2}$, $m_\perp$ is the transverse mass defined as:

$$m_\perp = \sqrt{E^2 - p_\perp^2} = \sqrt{m^2 + p_z^2} \tag{2}$$

[2]In fact there are three minimum bias triggers: Hits in the forward and backward regions, a minimal transverse energy cut and a random trigger.

[3]The detector is centred on the nominal interaction point, that is the centre of the extended region where the two proton beams intersect.

and η is the pseudorapidity

$$\eta = -\ln \tan(\theta/2) \tag{3}$$

where θ is the polar angle measured from the z-axis. The pseudorapidity is the rapidity y

$$y = \ln\left(\frac{E - p_z}{E + p_z}\right) \tag{4}$$

of a massless particle. Because the calorimeter measures the energy deposited in a certain direction, it is convenient to define the transverse energy:

$$E_\perp = E \sin(\theta) \tag{5}$$

which is the same as the transverse momentum for a massless particle. Distance in the $\eta \times \phi$ plane is given by $\Delta\mathcal{R}$:

$$\Delta\mathcal{R} = \sqrt{(\Delta\eta)^2 + (\Delta\phi)^2} \tag{6}$$

A definition considering y instead of η is currently being considered.

1.3 Detector

Figure 3 shows the ATLAS detector divided into it's four general components: the inner detector inside the solenoid magnet, the EM calorimeter, the hadronic calorimeter and the muon chambers inside the air-core toroidal magnet forming the outermost layer.

The inner detector covers the interval $|\eta| < 2.5$. The inner detector is contained by the solenoid magnet supplying a 2 T magnetic field to allow the inner detector to measure momentum. The inner detector contains silicon pixel, silicon strip and transition radiation detectors. The silicon pixel detector provides vertex resolution for charged particles to about 10 μm in the transverse plane and to about 100 μm along the beam axis. The silicon strip detector and transition radiation tracker follow particle motion in the magnetic field. This allows the measurement of particle momentum and the sign of the particle's charge.

The EM calorimeter is a liquid argon sampling calorimeter using lead absorber plates. It is

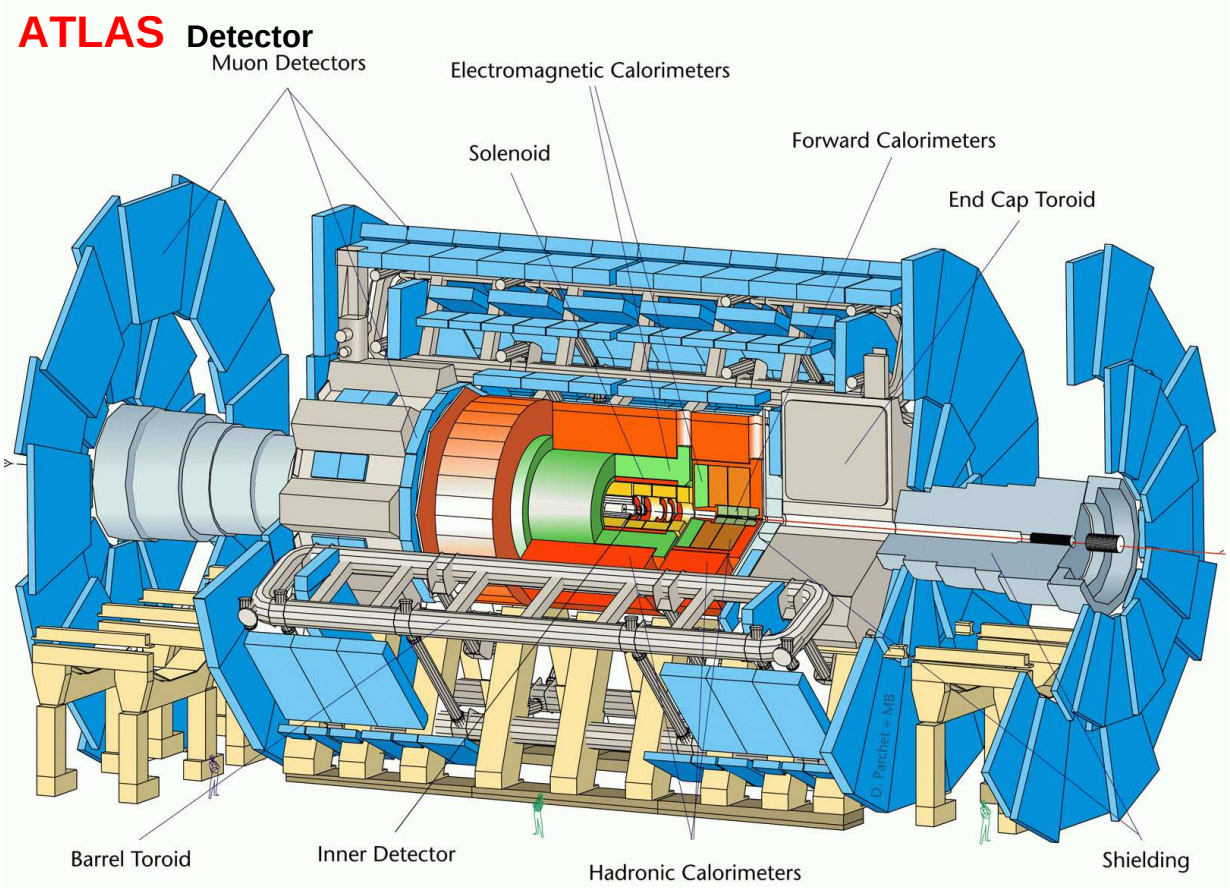

Figure 3: Schematic of the ATLAS detector layout. Note the scale given by the human figures.

divided into the barrel region covering $|\eta| < 1.475$ and the end-cap region extending the calorimeter coverage to $|\eta| < 3.2$. The EM calorimeter's accordion design allows for hermetic coverage in ϕ. The ATLAS calorimeters were designed to fully cover a large acceptance to measure the energy of most particles from the event. This means that a neutrino or an exotic particle leaving no signal in the detector causes *missing transverse energy* $\not{E}_\perp$ in the calorimeter.

The hadronic calorimeter surrounds the EM calorimeter. In the barrel region the hadronic calorimeter is a sampling calorimeter with scintillation plates read out by wavelength shifting fibres between layers of steel absorber. The barrel and extended barrel cover $|\eta| < 1.7$. The hadronic end-cap is a liquid argon sampling calorimeter employing copper absorber plates. It covers $2.5 < |\eta| < 3.2$. Finally the forward calorimeter is a sampling calorimeter employing liquid argon as active material and tungsten and copper as absorber. The forward calorimeter extends the pseudorapidity acceptance of the hadronic calorimeter to $|\eta| < \pm 4.9$. The calorimeter readout is segmented into layers of cells with a granularity of approximately $\eta \times \phi = 0.1 \times 0.1$ in the barrel and 0.2×0.2 in the end-cap region.

The calorimeters are surrounded by the toroidal magnet that gives ATLAS it's name. It deflects charged particles in air core magnets allowing momentum measurement of muons with the muon chambers. The barrel toroids cover the $|\eta| < 3$ region. The rest of the detector acceptance is covered by the end-cap toroids. Muons are detected by three sections of multilayer ionization chambers.

1.4 Calorimeters

Calorimeters measure the energy of particles which stop inside them. Electrons and photons incident on matter will produce a cascade of electrons and photons produced through bremsstrahlung and Compton scattering. Hadronic particles cause different cascade showers because nuclear interactions become important. The ATLAS calorimeters are non-compensating, that is they respond differently to hadrons than to electrons or photons. Figure 4 illustrates a hadronic shower. It is more complex than an electromagnetic shower. In the shower process electrons and photons are produced and deposit their energy as visible EM energy. Charged hadrons in the shower will also cause scintillation light in the tile calorimeter or ionization in the liquid argon yielding a vis-

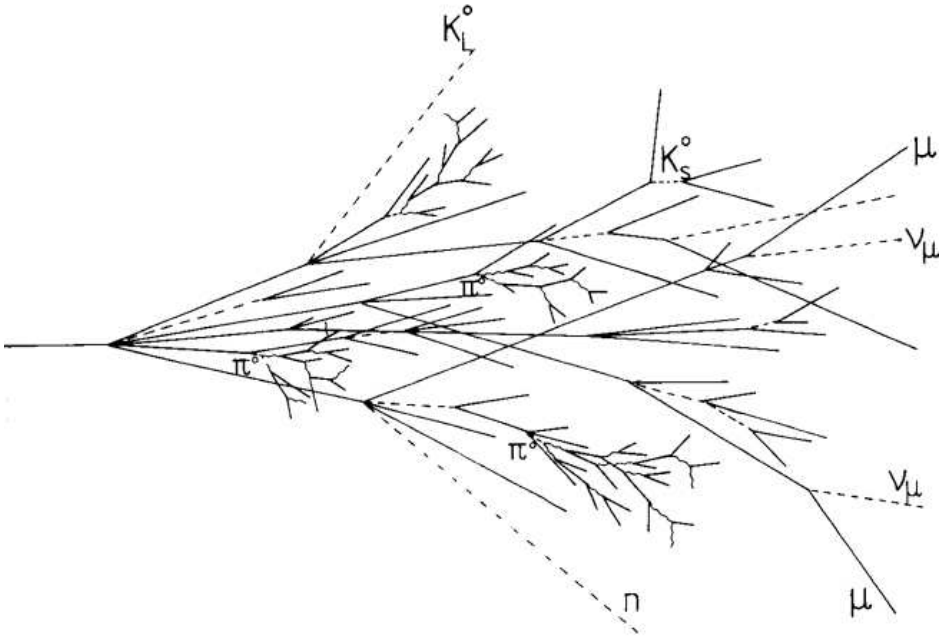

Figure 4: Schematic of a hadronic shower [4].

ible non-EM signal. Hadrons will also interact with the nuclei (mostly) in the absorber material causing some invisible non-EM component of the shower. Muons and neutrinos produced in the hadronic shower escape the calorimeter. Approximately 50% of the energy of the original hadron is the visible EM signal, around 25% is the visible non-EM signal, another 25% are deposited as invisible non-EM energy and about 2% escape the calorimeter. The exact proportion of each of these components depends on the energy of the original hadron and fluctuates significantly between showers.

A hadronic shower produces a different signal in the calorimeter than an EM shower. The hadronic calibration attempts to compensate for the difference in the calorimeter response to hadrons and electrons/photons such that the measurement for a hadron is the same as for an electron of the same energy. ATLAS is considering two approaches to the hadronic calibration: H1-style weights and local hadronic calibration. H1-style weights will be discussed in section 1.6 because they apply to jets, not to calorimeter objects. Local hadronic calibration is an attempt to separate the calibration of the hadronic signal deposited in the calorimeter, from the calibration of the physics object that produced the energy deposition.

Particles incident on the calorimeter produce a shower resulting in a signal in a group of neighbouring cells. The clustering algorithm described in appendix A identifies these groups of cells as clusters. Once the clusters are identified the cells in each cluster are weighted according to what type of cluster they occupy, the cluster energy, the cluster η and the cell energy density. Furthermore clusters around dead material regions (for example a cryostat wall) are calibrated to account for signal lost to uninstrumented parts of ATLAS. Finally each cluster is calibrated for energy deposited in the calorimeter which the clustering algorithm may have missed. The resulting clusters have been calibrated to hadronic scale.

1.5 Simulation & Reconstruction

There are two aspects to simulating data collection with ATLAS. First, the *pp* collisions supplied by the LHC must be generated, in particular the physics processes of interest must be generated. Second, the response of the ATLAS detector to the particles from the generated *pp* collision must be simulated.

Software tools for the generation of physics events and detector simulation yield files that emulate data. The ATLAS reconstruction software[4] is then run on the results of the detector simulation as if it were real collision events. Figure 5 displays that different particles interact differently with the parts of the detector. Generally electrons and photons will pass the tracker (electrons leaving a charged track in the inner detector) and deposit their energy in the EM calorimeter. Hadrons from the fragmentation of quarks will deposit some of their energy in the EM calorimeter and most in the hadronic calorimeter, and leave a track in the Inner Detector if the hadron is charged. Muons will leave a charged track in the Inner Detector, deposit little energy in the calorimeters also leaving a charged track in the muons chambers. Thus different algorithms are optimized to perform the reconstruction of electrons and photons, hadronic particles and muons. Each algorithm is run independently of the others. This means the same particle could be reconstructed as an electron by the EM algorithm and as a jet by the jet algorithm. In each event one must decide which reconstructed object to keep, and which to ignore.

[4]For the analysis presented in section 2 Athena version 12.0.6 was used.

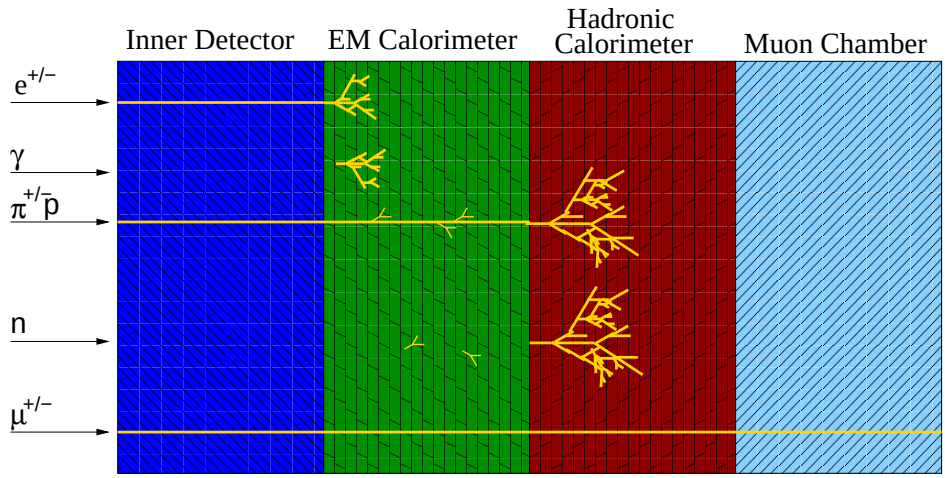

Figure 5: Schematic of particle interaction in different detector components.

1.6 Jets

Energetic quarks and gluons produced in a hard interaction cause a cascade of particles as they are scattered. Each quark (or gluon) forms a cascade of light hadrons (mostly pions). Exactly where and how this cascade begins is not well understood. To assess the uncertainty in jet simulation one usually models jets over a range of values for the QCD factorization and renormalization scales. The result of this cascade is a shower of hadrons in the direction of the original parton. These hadrons or their decay particles hit the calorimeter and initiate showers as displayed in figure 4. This evolution from hard scatter to calorimeter signal is displayed in figure 6.

As explained in section 1.4 the calorimeter signal may be grouped into clusters. Traditionally the cells are mapped onto $\eta \times \phi = 0.2 \times 0.2$ grid of towers. The goal is to associate groups of high energy cells, clusters or towers with the final state particles of the original hard scatter. A top-down algorithm is to identify all energy deposited in some cone opening from the interaction point into the detector with each of the particles from the original scatter. Bottom-up approaches define some distance between two cells, clusters or towers by their energies and distance in η and ϕ space and merge all within some distance of one another. Appendix B describes the most interesting jet algorithms used in ATLAS analysis.

Once the jets are determined from cells, towers or clusters not calibrated to the hadronic scale (via the local hadronic calibration described in section 1.4) the jets may be calibrated with H1-style

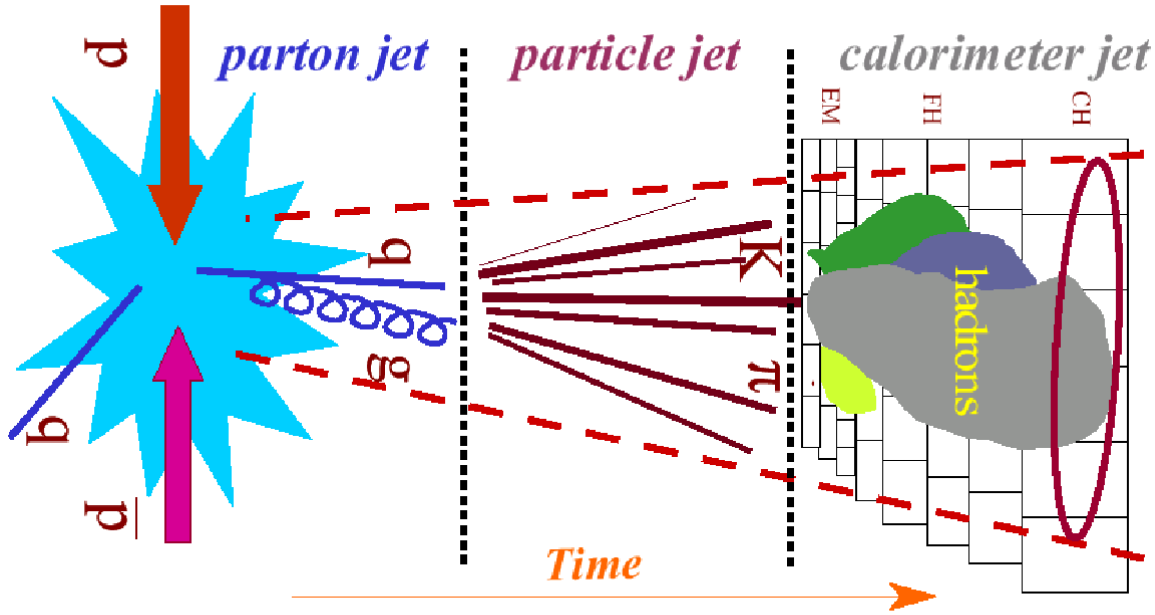

Figure 6: Schematic of jet evolution.

weights. The weights are determined by comparing the energy of reconstructed jets from a QCD simulation to the same jet algorithm run on the stable particles from the event generator. The jets are divided into regions of energy density; a weight depending on the energy density of each region is then applied to each part of the jet. The parameters of the weight function are determined by minimizing the difference between the weighted jet and the jet obtained from the stable particles from the generator [5]. The problem with this calibration approach is that it is dependent on the jet algorithm used, and the physics process used in the determination of the weights.

2 Jet Energy Scale Investigation

Jets calibrated to hadronic scale reflect the energy of all particles in the jet which hit the calorimeter. Charged particles with less that 350 MeV never reach the calorimeter and must still be accounted for. Muons and neutrinos produced in the decay of pions in the jet do not deposit their energy in the calorimeter. Particles from the fragmentation of the same parton may fall outside the

reconstructed jet. Different partons will fragment into jets differently. So these effects must be calibrated individually for the flavors of quarks and gluons. Particularly the heavy b-quark will form a B-meson which carries a larger fraction of the original parton momentum than mesons formed in the fragmentation of light quarks. A significant number of B-mesons decay into a lepton, it's neutrino and light mesons further changing the structure of the jet. Understanding the energy scale of b-jets is particularly important to find a low mass (< 135 GeV) Higgs.

To establish the jet energy scale one must investigate known physics processes in the early data taken by ATLAS. Photon reconstruction is more accurate than jet reconstruction. So events with a prompt photon recoiling against a jet can be used to calibrate jets by requiring the jet and photon transverse momenta to balance. The same event with a Z-boson instead of the photon permits the same approach if the Z decays into leptons. Another approach is to look at the QCD scatter of two quarks or gluons resulting in two jets in the detector, and requiring their transverse momenta to balance.

The decay of known particles provides a different scaling approach. The jet energy scale may be established with the decay of a W-boson into two jets, forcing the jet 4-momenta to reconstruct the mass of the W. Selecting the W decaying to two jets from QCD background is hard. Top pairs provide both the decay of a W-boson into quarks and a kinematic signature that allows a strong rejection of the QCD background. Study of top quarks decays also allows the calibration of b-jets.

2.1 Semi-Leptonic Top Events

Top pairs (or $t\bar{t}$ events) will be abundant at the LHC with an estimated cross-section[5] of 833^{+52}_{-39} pb [6]. Figure 7 displays the leading order diagrams for top pair production in proton-proton collisions. At 14 TeV the fraction of the proton's momentum necessary to form a top pair is quite low and the gluon fusion diagram of figure 7 dominates the production cross-section. Almost all top quarks decay into a W-boson and a b-quark. 32.12% of all W-bosons decay into a lepton and it's neutrino (ie. leptonically) while 67.60% decay into two quarks (ie. hadronically) [7]. Figure 8 shows the semi-leptonic decay of a top pair: one W-boson decays leptonically and the other hadronically.

[5]The 833^{+52}_{-39} pb cross-section for $t\bar{t}$ events is calculated next-to-leading order with next-to-leading logarithmic correction for higher order diagrams.

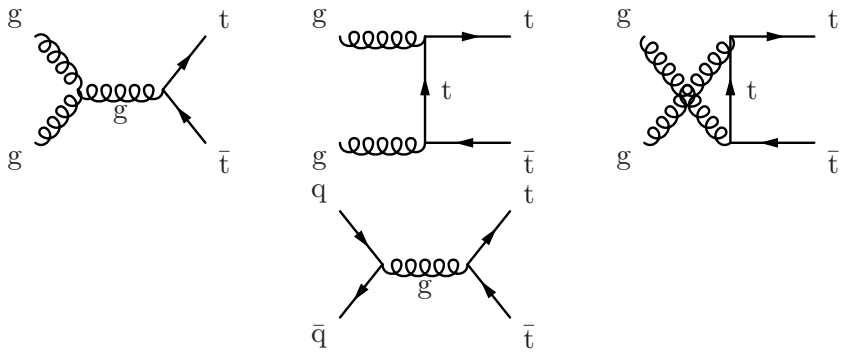

Figure 7: Leading order top pair production diagrams.

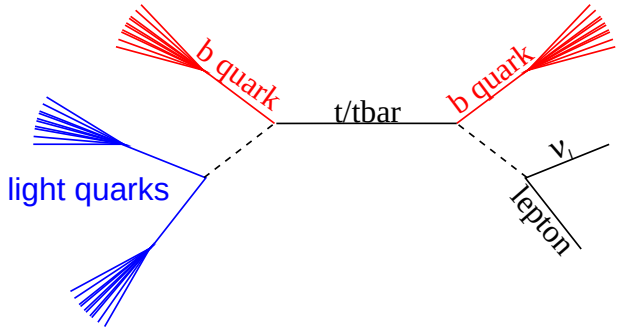

Figure 8: Schematic of a semi-leptonic top event.

Semi-leptonic decays provide a lepton and missing transverse energy (from the neutrino) which can be used to reduce the QCD background. The other W provides two light jets to establish the light jet energy scale. Since there is no data from ATLAS yet, 1 fb^{-1} of top events were simulated requiring that at least one W decays leptonically. The cross-section for this sample of events is estimated to be 452 pb.

To select data for our analysis we require one of two triggers: either an energetic electron or muon[6]. Almost all the semi-leptonic $t\bar{t}$ decays pass this selection.

Particles found by the reconstruction software must be selected for the analysis before selecting the $t\bar{t}$ events. Electrons that were reconstructed by the algorithm for EM-particles[7] are selected first. If these electrons came from the decay of a W they likely have a large transverse momentum; the electrons are required to have 20 GeV of transverse momentum. Information from the tracker is needed to discriminate electrons from photons. So the electron must traverse the tracker ($|\eta| < 2.5$).

[6]The inclusive EM25 trigger for the electron or MU20 or MU40 trigger for the muon [8].
[7]As identified by the isEM bit in the analysis software.

Electrons in the region between the barrel and end-cap calorimeters ($1.35 < |\eta| < 1.57$) are rejected because the energy measurement in that region is inaccurate. The electron must be isolated; this removes leptons found in jets. An electron is isolated if the energy deposited in the calorimeter around the electron track is small compared to the transverse momentum of the electron[8]. To avoid overlap with muons and jets erroneously reconstructed by the muon and jet algorithms all muons and jets reconstructed within $\Delta\mathcal{R} < 0.2$ of the remaining electrons are removed.

Muons[9] from a W-boson likely have a high transverse momentum; the muon must have at least 20 GeV of transverse momentum. Tracker information is required for a good transverse momentum measurement so the muon must traverse the tracker ($|\eta| < 2.5$). No jets may contain the muon to cut the muons often produced by the B-meson decay in b-jets[10].

Finally the jets are selected. The b-jets from the top decays and the light jets from the W decay likely have a large transverse momentum; jets must have at least 20 GeV of transverse energy. For jets the energy measurement by the calorimeter is much more accurate than the jet momentum measurement from it's charged tracks by the tracker. So the cut for jets is on the transverse energy. Jets must be inside the tracker ($|\eta| < 2.5$) to allow b-tagging information to be added to the analysis in the future. The top analysis was developed using cone jets with opening angle $\Delta\mathcal{R} = 0.4$ built from calorimeter towers and calibrated to hadronic scale[11]. Those jets were chosen because they are widely used in ATLAS physics analysis. The top events will be used to determine the jet energy scale which is required for all calorimeter calibration schemes and jet algorithms. In fact the analysis has been tested on jets built from calorimeter clusters instead of towers. The results are almost identical and will not be displayed here.

$t\bar{t}$ events are selected from this well defined set of leptons and jets. A semi-leptonic top decay is required to produce one and only one good lepton (either an electron or a muon, tauons are ignored) and at least 20 GeV of missing transverse energy from the recoiling neutrino. The event must also have four jets: At least three jets with $E_\perp > 40$ GeV and a fourth jet with $E_\perp > 20$ GeV.

[8] For an electron to be isolated $E_\perp$ of all calorimeter cells within $\Delta\mathcal{R} < 0.4$ and $\Delta\mathcal{R} < 0.2$ of the electron is less than 0.20 and 0.07 times the electrons $p_\perp$, respectively.

[9] As reconstructed by the Muid algorithm.

[10] $\Delta\mathcal{R}$ from the muon to the closest jet must be greater than 0.4 for cone jets with an opening angle of $\Delta\mathcal{R} = 0.4$.

[11] Using H1-style weights.

Cut	$t\bar{t}$ Events	Remaining
No Cuts:	433554	100.0%
Lepton cut:	160546	37.0%
$\not{E}_\perp$ cut:	145712	33.6%
Jet cut:	56119	12.9%

Table 1: Cut flow for $t\bar{t}$ selection on 1 fb^{-1} of simulated LHC events.

The lepton and missing transverse energy cut greatly reduce the QCD background. Table 2.1 shows the cut flow for top events. The jets from the hadronic top and W decay must be identified. To select the jets each subset of four jets[12] of all good jets in the event is considered. The three jets with the highest triplet transverse momentum are assigned to the hadronic top. The left over jet is identified as the b-jet of the leptonic top. Next, the two jets in the hadronic top hypothesis with the highest doublet transverse momentum are identified as the light jets. The mass measurement from this assignment is displayed in figures 9 and 10. The signal to noise ratios are 41.5% and 12.8% for the top quark and W-boson hypothesis respectively. The background is caused by choosing the wrong jets for the hadronic top and W hypothesis. The b-jet from the hadronic top misidentified as one of the light jets causes the broad background peak visible in figure 10. The remaining background for the top and W hypothesis arises in equal parts from the b-jet of the leptonic top and background jets from the underlying event contaminating the hadronic top and W hypothesis. Di-leptonic $t\bar{t}$ decays and semi-leptonic $t\bar{t}$ decays involving a tauon passing the cuts account for 5.7% and 6.8% of the background. Other physics processes such as W-boson production and QCD events are small backgrounds [9]. The three and two-jet mass in figures 9 and 10 come from top events simulated with $M_{\mathrm{t}} = 175$ GeV and $M_{\mathrm{W}} = 80.4$ GeV. The fit in figure 9 is offset because of the b-jet energy scale. The width of the peak reflects the top quark's decay width and the detector resolution. The fit in figure 10 returns a value very close to the simulated W-boson mass. This means that the H1-style weights perform well on light jets in top events.

This reconstruction is of simulated events so the 4-momenta of the quarks and leptons from the $t\bar{t}$ decay are known. That information can be used to assess how well the hypothesis selection

[12] At least three of which have $E_\perp > 40$ GeV and the fourth has $E_\perp > 20$ GeV.

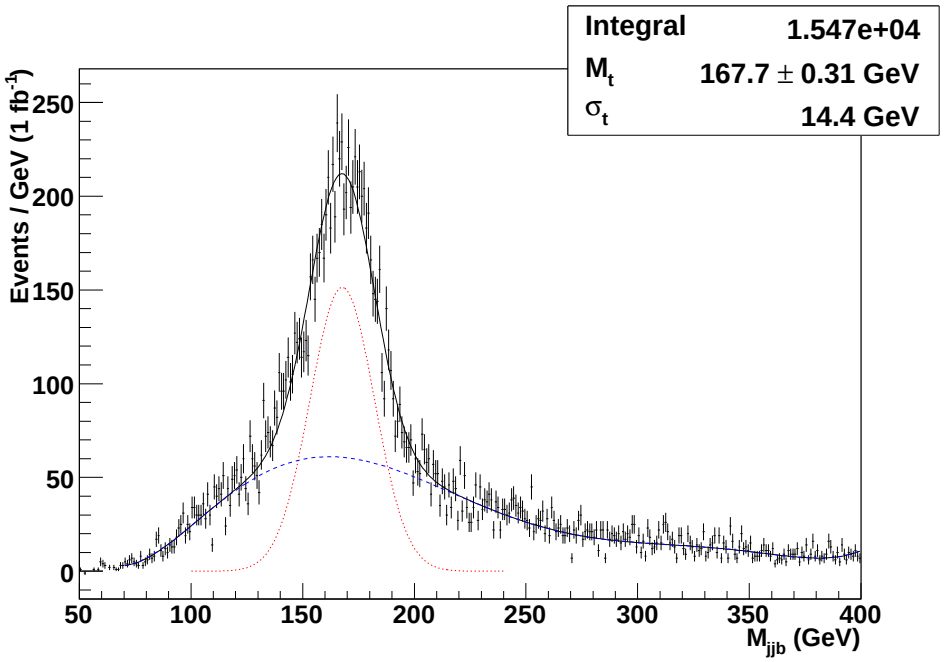

Figure 9: The measured three-jet mass from the hadronic top hypothesis. The peak is fit with a Gaussian (red dotted line) and the background is modelled using a 7^{th} order Chebychev polynomial (blue dashed line). The mass is measured from the combined fit (black line) $M_{\mathrm{t}} = 167.7$ GeV. The integral gives the number of events in the histogram.

Hypothesis	Events	Truth Matched	Efficiency
Hadronic Top	30234	7098	23%
Hadronic W	30234	5307	17%

Table 2: Selection efficiency of commissioning hypothesis for three-jets matched to the hadronic top or the two-jets matched to the hadronic W decay. Only hypotheses which had all four jets matched to a quark (44% of all hypotheses) are considered.

performs. First the reconstructed jets are mapped to the quarks. Each quark is associated to all jets within $\Delta\mathcal{R} = 0.2$. The closest associated jet is mapped to the quark. The hadronic top hypothesis is considered to be matched by the truth if the three quarks from the hadronic top are matched to the three jets in the hadronic top hypothesis. Similarly the hadronic W hypothesis is considered to be matched by the truth if the two quarks from the hadronic W are matched to the two jets in the hadronic W hypothesis. Table 2 illustrates the efficiency of the hypothesis selection described above for identifying the hadronic top and W-boson.

The fit in figure 9 is constructed by filling a histogram with the three jet masses of all truth

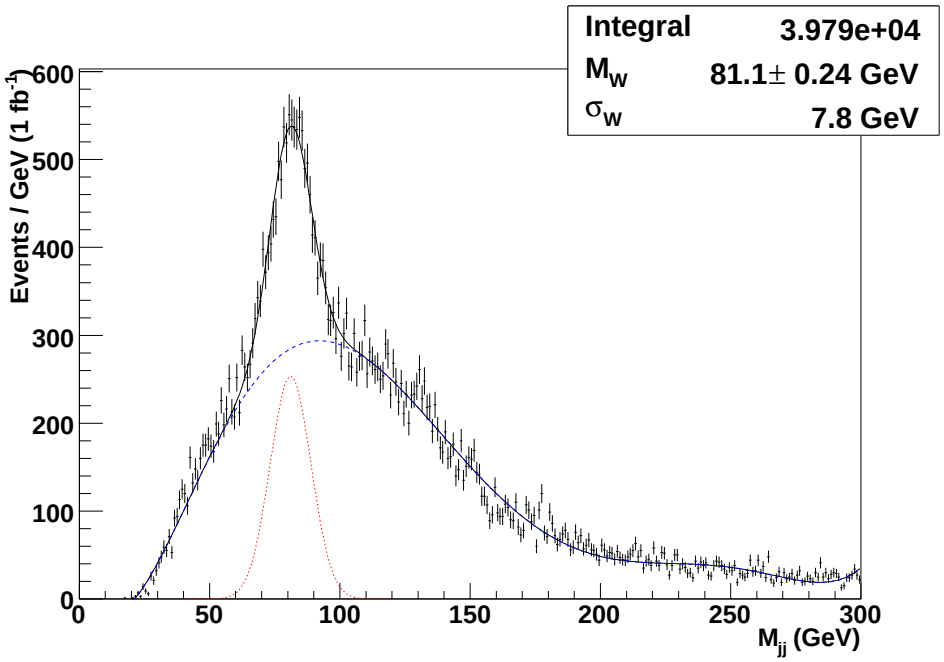

Figure 10: The measured two-jet mass from the hadronic W-boson hypothesis. The peak is fit with a Gaussian (red dotted line) and the background is modelled with a 7^{th} order Chebychev polynomial (blue dashed line). The mass is measured from the combined fit (black line) $M_{\mathrm{W}} = 81.1$ GeV. The integral gives the number of events in the histogram.

matched hadronic top hypotheses. This histogram is fit with the signal shape. Another histogram is filled with the three-jet mass of all hadronic top hypotheses which failed the truth matching. This histogram is fit with the background shape. The parameters from these signal and background fits are used as the starting point for the fit to the histogram of all hypotheses. The same procedure is used for the two-jet mass histogram in figure 10.

2.2 Iterative Approach

The iterative approach to find the light jet scale was adopted from D. Pallin [10]. To determine the light jet energy scale the measured W-boson mass is compared to the known W mass. The sum of the two quark 4-momenta corresponds to the known W[13] and the sum of the two jet 4-momenta corresponds to the measured W:

$$\frac{M_{\mathrm{W}}}{M_{\mathrm{W}}^{\mathrm{ex}}} = \sqrt{\frac{(p_{\mathrm{q1}} + p_{\mathrm{q2}})^2}{(p_{\mathrm{j1}} + p_{\mathrm{j2}})^2}} \tag{7}$$

[13] Assuming that the decay width of the W may be neglected compared to detector effects.

where M_{W} and $M_{\mathrm{W}}^{\mathrm{ex}}$ are the known and measured W mass, respectively. p_{q1} and p_{q2} are the 4-momenta of the two quarks and p_{j1} and p_{j2} are the 4-momenta of the two jets. To extract the energy scale jets are assumed to be massless and equation 7 becomes:

$$\frac{M_{\mathrm{W}}}{M_{\mathrm{W}}^{\mathrm{ex}}} \approx \sqrt{\frac{E_{\mathrm{q1}} \cdot E_{\mathrm{q2}}}{E_{\mathrm{j1}} \cdot E_{\mathrm{j1}}} \cdot \frac{1-\cos\theta^{\mathrm{q}}}{1-\cos\theta^{\mathrm{j}}}}$$

where E_{q1} and E_{q2} are energies of the two quarks and E_{j1} and E_{j2} are the energies of the two jets. θ^{q} is the angle between the quarks and θ^{j} is the angle between the jets. If we also assume that the measured jet angles are correct we have:

$$\frac{M_{\mathrm{W}}}{M_{\mathrm{W}}^{\mathrm{ex}}} \approx \sqrt{\frac{E_{\mathrm{q1}}}{E_{\mathrm{j1}}} \cdot \frac{E_{\mathrm{q2}}}{E_{\mathrm{j2}}}} = \sqrt{f(E_{\mathrm{j1}}, \eta_{\mathrm{j1}}) f(E_{\mathrm{j2}}, \eta_{\mathrm{j2}})} \tag{8}$$

Where $f(E, \eta)$ is the light jet energy scale for a jet of energy E at pseudorapidity η. The mass ratio is filled into a histogram for the two jet E and η for each event. The jet energy scale is then applied to the 4-momentum of each jet:

$$p' = f(E, \eta) \cdot p$$

A new scale is then determined from the calibrated jets and so on. The procedure converges after five iterations. Figure 11 displays the resulting jet energy scale after each iteration. The result is compared to the effective jet energy scale $\sqrt{\frac{E_{\mathrm{q1}}}{E_{\mathrm{j1}}} \cdot \frac{E_{\mathrm{q2}}}{E_{\mathrm{j2}}}}$ obtained from truth matching.

The iterative procedure does produces a stable result regardless of the initial jet energy scale assumed. A flat distribution with a jet energy scale of unity is chosen for the seed, but inserting the true or effective energy scale produces the same result.

The difference between the iterative result and the effective jet energy scale may be attributed to the assumptions made for the iterative procedure because: (a) jets have a significant mass (which is in part an artifact of the jet reconstruction) and (b) the angle between jets does not reflect the angle between the quarks. The uncertainty in the difference between the effective and the iterative result in figure 11 (b) must be understood to extract the jet energy scale using the iterative method.

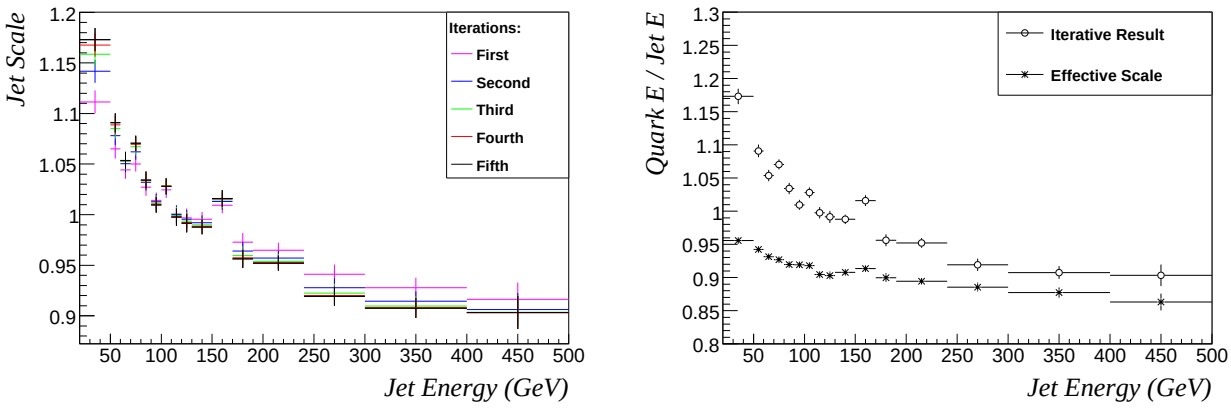

(a) (b)

Figure 11: (a) The iterative jet energy scale algorithm converges after a few iterations. (b) The light jet energy scale as a function of jet energy as determined by the iterative procedure. The effective energy scale is calculated as $\sqrt{\frac{E_{q1}}{E_{j1}}\frac{E_{q2}}{E_{j2}}}$.

Recall that this energy scale only applies to light jets.

2.3 Kinematic Fit Approach

Figure 8 shows the kinematic signature of a $t\bar{t}$ event which provides some constraints on the measured jets. The iterative approach used the knowledge that the two light jets were produced by the decay of a W-boson. The two light jets and the b-jet from the hadronic top came from the decay of a top quark. Thus the three jet 4-momenta must add up to the top 4-momentum. The information from the leptonic top provides some further constraints. The leptonic W-boson decay produces the lepton and the missing transverse energy. The lepton, missing energy and last b-jet are the decay products of the leptonic top.

The light and b-jet energy scale are determined by forcing the known top and W mass to be reconstructed. For each event we define

$$\chi^2_{\text{kine}} = \sum^{\{\text{had, lep}\}} \left(\left[\frac{M_{\text{W}} - M^{\text{ex}}_{\text{W}}}{\Gamma_{\text{W}}} \right]^2 + \left[\frac{M_{\text{t}} - M^{\text{ex}}_{\text{t}}}{\Gamma_{\text{t}}} \right]^2 \right) \tag{9}$$

where M_{W} and M_{t} are the known W and top mass, Γ_{W} and Γ_{t} are the known W decay width and top decay width as calculated by the standard model prediction [11]. M^{ex}_{W} and M^{ex}_{t} are the

reconstructed two-jet and three-jet mass from the W and top hypothesis. In the calculation of the leptonic W and top mass the transverse momentum of the neutrino is taken to be the missing transverse energy and the longitudinal momentum of the neutrino is allowed to vary freely.

The fit is further constrained by the detector resolution:

$$\chi^2_{\rm det} = \sum_{i}^{\rm Light\ Jets} \left[\frac{E_i(1-f_\ell(E_i,\eta))}{\sigma_{\rm jet}(E_i,\eta)}\right]^2 + \sum_{i}^{\rm B\ Jets} \left[\frac{E_i(1-f_b(E_i,\eta))}{\sigma_{\rm jet}(E_i,\eta)}\right]^2 + \left[\frac{\not\!\!E_\perp(1-\alpha)}{\sigma_{\not\!\!E_\perp}(H_\perp)}\right]^2 \qquad (10)$$

where E_i is the jet energy of jet i. f_ℓ and f_b are the light and b jet energy scale. $\sigma_{\rm jet}$ is the jet energy resolution obtained using a two-jet balancing method [12]:

$$\frac{\sigma_{\rm jet}(E_\perp)}{E_\perp} = \frac{0.6}{\sqrt{E_\perp}} \oplus \frac{5.7}{E_\perp} \oplus 0.041$$

where $E_\perp$ is in GeV. The jet energy resolution is taken to be the same of light and b-jets. $\not\!\!E_\perp$ is the missing transverse energy, α is the $\not\!\!E_\perp$ scale and $H_\perp$ is the scalar sum of the transverse energy in each cell of the calorimeter. $\sigma_{\not\!\!E_\perp}(H_\perp)$ is the $\not\!\!E_\perp$ resolution which may be derived from the resolution on the x and y components of the $\not\!\!E_\perp$ assuming that the two are not correlated:

$$\sigma_{\not\!\!E_\perp}(H_\perp) = \sigma_{\not\!\!E_x}(H_\perp) = 0.57\sqrt{H_\perp}$$

where $\sigma_{\not\!\!E_x} = \sigma_{\not\!\!E_y} \approx 0.57\sqrt{H_\perp}$ is the resolution on the x and y component of the missing transverse energy and $H_\perp$ is in GeV [13]. The full $\chi^2 = \chi^2_{\rm kine} + \chi^2_{\rm det}$ is minimized using MINUIT [14] for each top event. The resulting coefficients for each jet are recorded if the minimization converged.

Figure 12 shows that the resulting light jet energy scale calculated from jets within some energy and pseudorapidity range. The light jet energy scale background is contaminated by b-jets and vica-versa if the hadronic W hypothesis is incorrect. Both jet energy scales are slightly effected by background jets in the hypothesis.

Both the signal and background shapes in figure 12 were fit with a Gaussian around the peak of the jet energy scale distributions. The background peaks in the same region as the signal. The high energy (above 300 GeV) range lacks sufficient statistics to determine the jet energy scale. That

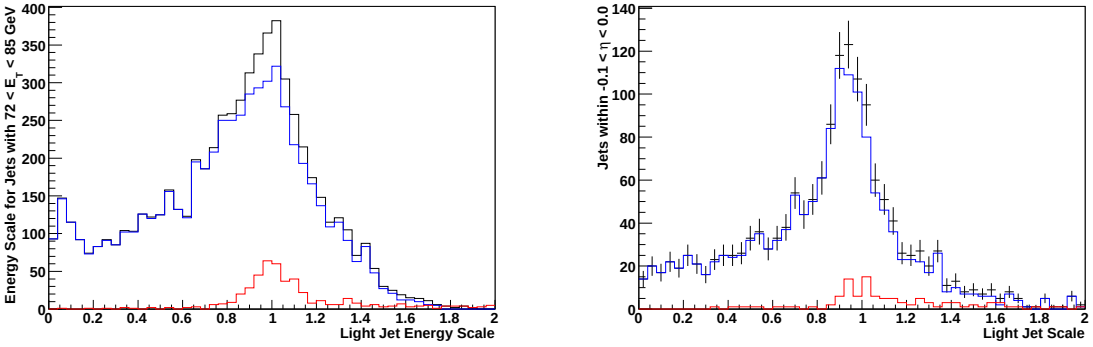

(a) (b)

Figure 12: The jet energy scale from χ^2 fit for jets with (a) transverse energy $72 < E_\perp < 85$ GeV or (b) pseudorapidity $-0.1 < \eta < 0.0$. The signal is in red, the combinatorial background in blue.

means top events will supply a jet energy scale to about 300 GeV.

2.4 Bootstrapping

The physics goal of my thesis is a measurement of quark compositeness which requires the measurement of very energetic jets (a few TeV). This means the jet energy scale from the top analysis must be extended to higher energy. No known Standard Model particle will decay into jets of a few TeV of transverse momentum, so one of the other approaches must be used.

In next-to-leading order diagrams of QCD two-jet events one scattered parton may radiate one or more gluons which form their own jets. Figure 13 shows this event topology. The transverse momentum of one very energetic jet is balanced by a few lower energy jets. Before the jet energy scale derived from tops may be used it must be shown that the top jet energy scale also applies in QCD two-jet events. The jet energy scale from top events can be tested in QCD events by applying the jet energy scale from top events to low energy two-jet events and testing the transverse momentum balance.

Table 3 shows that very energetic jets are rare. For example a two-jet event resulting in jets with over 2 TeV will occur around 6 times per year at $\mathcal{L} = 10^{31}$ cm^{-2}s^{-1} of luminosity. This means it will take time to establish the jet energy scale to a few TeV.

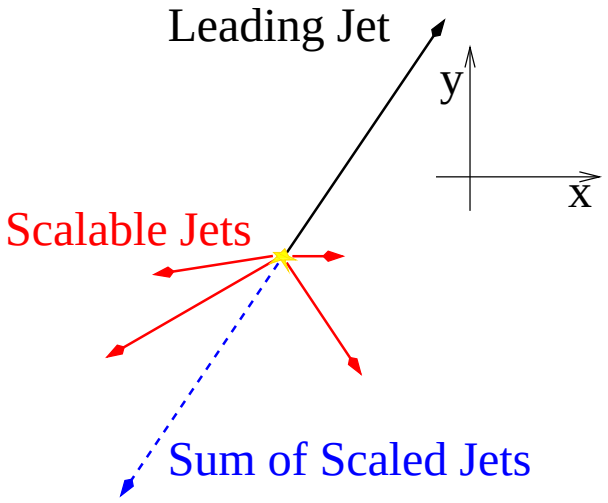

Figure 13: Schematic of QCD event suitable for bootstrapping

Sample	$E_\perp$ Range	Cross-Section	Approx. Rate
J0	10 – 17 GeV	17.49 mb	200 kHz
J1	17 – 35 GeV	1.377 mb	10 kHz
J2	35 – 70 GeV	96.3 μb	1 kHz
J3	70 – 140 GeV	6.135 μb	50 Hz
J4	140 – 280 GeV	316.8 nb	3 kHz
J5	280 – 560 GeV	12.47 nb	0.1 kHz
J6	560 – 1120 GeV	344.5 pb	3 mHz
J7	1120 – 2240 GeV	5.3 pb	50 μHz
J8	$>$ 2240 GeV	22.2 fb	0.2 μHz

Table 3: Two-jet cross-sections from the Pythia generator [15]. The approximate rate is calculated for low luminosity ($10^{31}\text{cm}^{-2}\text{s}^{-1}$) LHC operation.

3 Research Plans

The LHC will soon produce pp collisions at 14 TeV. These will allow the exploration of physics theories beyond the Standard Model. Predictions of the Standard Model such as the existence of the Higgs boson will be tested by ATLAS. Furthermore ATLAS will look for the predictions of new theories such as supersymmetry, extra dimensions or technicolour. From past experience it is reasonable to assume that some of, or perhaps all, the fundamental particles of the Standard Model are in fact composite particles.

The first such test of compositeness was Rutherford's gold foil experiment [16]. The atomic structure of gold effected how alpha particles were scattered off a gold foil. The momentum transferred between the alpha particle and the gold nucleus is much larger than what would be allowed if the atom were an extended (10 Å) particle. Analogously if the quark is made of more fundamental particles (referred to as preons) this would change the spectrum of particles scattered off quarks. This change is described as a structure function for the quark:

$$F(Q^2) = \left(1 - \frac{Q^2}{\Lambda^2}\right)^{-1}$$

where Q is the 4-momentum transferred, and Λ is the energy at which the structure of the quark becomes apparent [17]. The momentum and angular spectrum of the scattered particles (in this case jets) reflects the structure of the quarks in the collision. So compositeness will change the inclusive jet cross-section, the angular distribution, and the two-jet mass spectrum because of new interactions, as sketched in figure 14. The 4-quark vertex interactions (figure 14 (b) and (c)) add a term to the Standard Model Lagrangian which becomes important at the compositeness scale Λ:

$$\mathcal{L}_{\text{comp}} = \frac{Ag^2}{2\Lambda}\left(\sum_{\text{quarks}} \bar{q}_{\text{L}}\gamma^{\mu}q_{\text{L}}\right)\left(\sum_{\text{quarks}} \bar{q}_{\text{L}}\gamma_{\mu}q_{\text{L}}\right)$$

where $A = \pm 1$ determines whether the effect of the new terms is constructive (+) or destructive (−), $g^2/4\pi = 1$ is the coupling strength of interactions between preons and the sums run over all the quarks with structure. The CDF and DØ collaborations at the Tevatron searched for compositeness

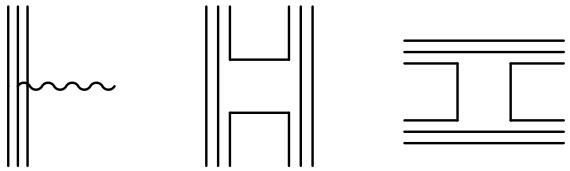

(a) (b) (c)

Figure 14: Effects allowed once the momentum transfer between quarks becomes comparable to the compositeness scale Λ. Preons will result in (a) structure functions changing quark interaction as well as allowing the 4-quark vertexes displayed in (b) and (c).

in the measured inclusive jet cross-section, angular distribution and two-jet mass spectrum using 2 TeV $p\bar{p}$ collisions. The results from CDF and DØ will be presented in the relevant sections below.

3.1 Systematics

The sources of systematic error may be divided into experimental and theoretical uncertainties. The most important experimental problems arise from the calorimeter response. Different technologies used in different calorimeter regions require individual calibration. The ATLAS calorimeters are non-compensating: each calorimeter has a different response to hadrons and to electrons (e/h). Furthermore energy is lost in regions between different calorimeters. More energy is lost for very high energy jets which extend beyond the calorimeter. Jet calibration is complex because jets often stretch across multiple calorimeter regions and the calibration must account for all these effects. Some low energy particles in each jet never reach the calorimeter due to the magnetic field in the tracker volume. More energy is lost to muons and neutrinos (produced in the jet) which do not deposit their energy in the calorimeter. The in-situ jet energy scale from section 2 accounts for the effects not properly handled in the calorimeter calibration. A miscalibration of the jet energy scale will fake a compositeness signal as discussed in the following sections. So the jet energy scale must be understood over the entire energy range of measured jets to detect compositeness. The jet energy scale from top events may not be valid for jets for QCD interactions because underlying event will differ from event type to event type. The trigger efficiency for jet events and the knowledge of the total luminosity must also be considered for any compositeness measurement.

The theoretical uncertainty reflects the limited knowledge of the parton distribution functions

for the proton in most of the kinematic range of the LHC and the uncertainty in jet fragmentation. The distribution of the proton's momentum among it's constituents directly determines the number of partons scatted at any given energy and angle. The uncertainty in the gluon distribution function at low momentum fraction x is particularly important because gluon fusion diagrams are dominant at the high energy collisions needed for the compositeness measurement.

The modelling of the jet fragmentation is important because the jet algorithm used becomes involved when trying to calculate the expected cross-section to next-to-leading order. The jet simulation must be tuned to properly model for two of the three scattered partons merging into one jet. Two partons scattered within $\mathcal{R}_{\text{sep}} \times \Delta\mathcal{R}$ for jets with opening angle $\Delta\mathcal{R}$ and some choice for $\mathcal{R}_{\text{sep}}$ are merged by the jet simulation. CDF and DØ have chosen to merge any two partons scattered within $\mathcal{R}_{\text{sep}} = 1.3$ times the opening angle of the cone algorithm[14]. The renormalization and factorization scale (usually taken to be one and the same) further affect the simulation of jets. These scales are usually varied over a range of the observed jet energies to assess the uncertainty in jet simulation.

3.2 Inclusive Jet Cross-Section

The new interactions allowed for composite quarks will change the inclusive jet cross-section at energies high enough to reveal the preons. Figure 15 shows the expected $E_\perp$ spectrum of the leading two jets expected by the Standard Model and compositeness at different scales. The plots were made with 30 fb^{-1} of simulation for QCD, γ^*/Z, W and $\mathrm{t\bar{t}}$ processes resulting in qq, qg, gg, $g\gamma$, $q\gamma$ and $\gamma\gamma$ final states. The interaction between partons must have carried at least 600 GeV for the event to be passed on the ATLAS simulation and reconstruction. The effect of the compositeness interactions is taken to be constructive in the Lagrangian.

The inclusive jet cross-section is dependent first on the knowledge of the momenta of the partons from the protons entering into the collisions. Because most interactions at the LHC will come from gluon fusion the uncertainty in the CTEQ [1] and MRSA [19] models for the gluon distribution function is a significant error. The dominant experimental issue is the linearity of the jet energy

[14] CDF and DØ adopted cones with a $\Delta\mathcal{R} = 0.7$ opening angle as default.

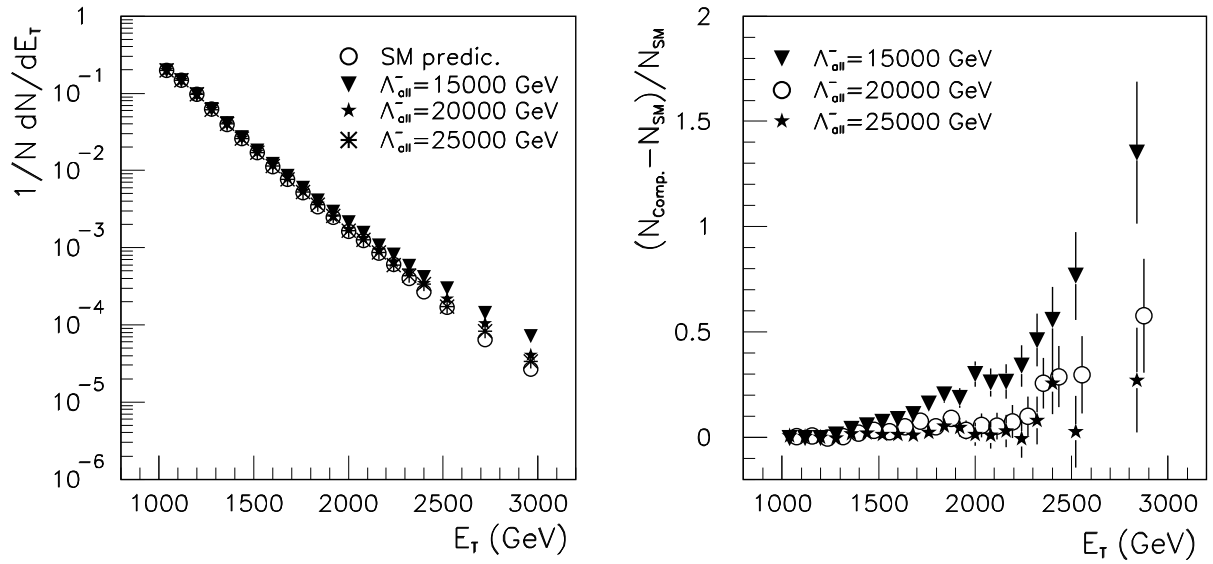

(a) (b)

Figure 15: The E_T distribution of (a) the inclusive jet cross-section and (b) difference between the QCD and compositeness predictions for the inclusive jet cross-section. The error bars in each plot correspond to 30 fb^{-1} of data [18].

scale at high energy.

The effect of the uncertainty in the parton distribution functions on the inclusive jet cross-section is displayed in figure 16. The range plotted here is established by simulating the QCD jet spectrum using CTEQ4, MRS and GRV94 as the PDF. Figure 17 shows the effect of a non-linearity in the jet energy scale.

To make a final statement on the certainty level of the compositeness measurement one determines the number of excess events measured above some energy threshold E_{T}^0 as compared to the excess events predicted by the Standard Model:

$$R = \left(\frac{N(E_\perp > E_\perp^0)}{N(E_\perp < E_\perp^0)}\right)_{\mathrm{comp}} \cdot \left(\frac{N(E_\perp > E_\perp^0)}{N(E_\perp < E_\perp^0)}\right)_{\mathrm{SM}}^{-1} \tag{11}$$

CDF and DØ have measured the inclusive jet cross-section excluding compositeness models at $\Lambda \leq 450$ GeV (4×10^{-4} fm) with 95% certainty [2, 20]. With 30 fb^{-1} of integrated luminosity ATLAS could measure compositeness at $\Lambda \leq 25$ TeV [18]. The inclusive jet cross-section is an

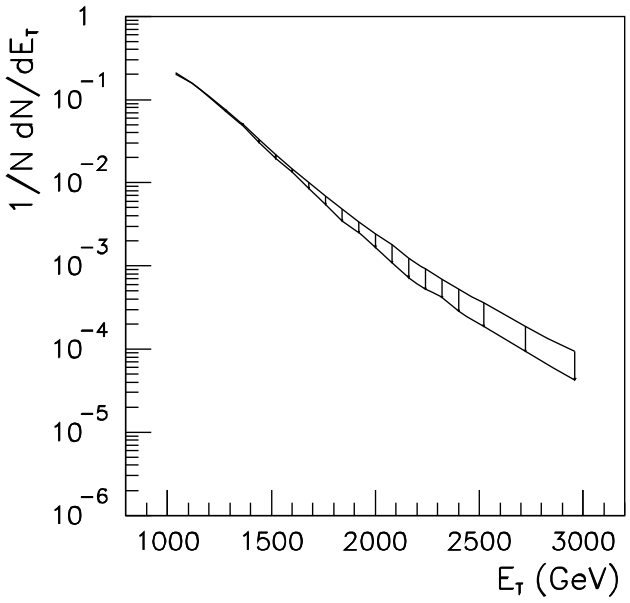

Figure 16: The effect of uncertainties in the parton distribution function on the inclusive jet cross-section [18].

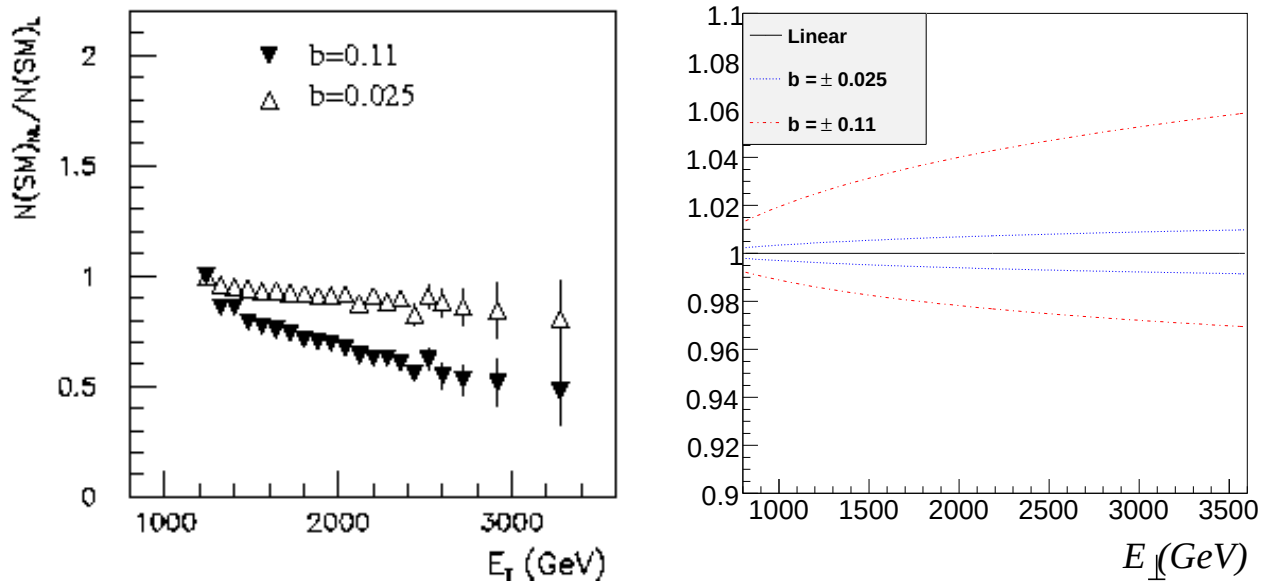

(a) (b)

Figure 17: (a) The effect of non-linearity in the jet energy scale on the inclusive jet cross-section [18] and (b) corresponding uncertainty in jet energy scale.

important test of QCD regardless of finding evidence for compositeness.

3.3 Two-Jet Angular Distribution

The angular distribution of jets is sensitive to compositeness and resilient to non-linearity in the jet energy scale. For compositeness searches the longitudinal angle between the two leading jets is written as:

$$\chi = e^{|\Delta\eta|}$$

where $\Delta\eta$ is separation of the two leading jets in pseudorapidity. It may be more illuminating to write χ in terms of the centre of momentum angle between the two leading jets Θ^* for two-jet events:

$$\chi = \frac{1 + |\cos\Theta^*|}{1 - |\cos\Theta^*|}$$

Figure 18 shows that compositeness models predict an excess of jets at low χ, that is an excess of events in which the two jets are not back-to-back. This is particularly apparent for high two-jet masses.

Again the two main sources of error are the parton distribution functions and the jet energy scale. To show the error introduced by the PDF we define a ratio similar to equation (11), but this time with a maximum value of χ rather than a minimum of $E_\perp$. Figure 19 shows the compositeness prediction compared to the Standard Model prediction using different PDFs and the effect of non-linearity in the jet energy scale. Previous measurements of the two-jet angle by CDF and DØ have ruled out (with 95% confidence) compositeness at $\Lambda \leq 1.8$ TeV (10^{-19} fm) for constructive interference and $\Lambda \leq 1.6$ TeV for destructive interference from the new interactions [21, 22]. With 1 fb^{-1} of data ATLAS will be able to detect compositeness at 14 TeV using the two-jet angular spectrum.

3.4 Two-Jet Mass Spectrum

The two-jet mass spectrum is sensitive to many new physics signatures. The new interactions permitted in compositeness models are only one of these signatures. Assuming jets are massless

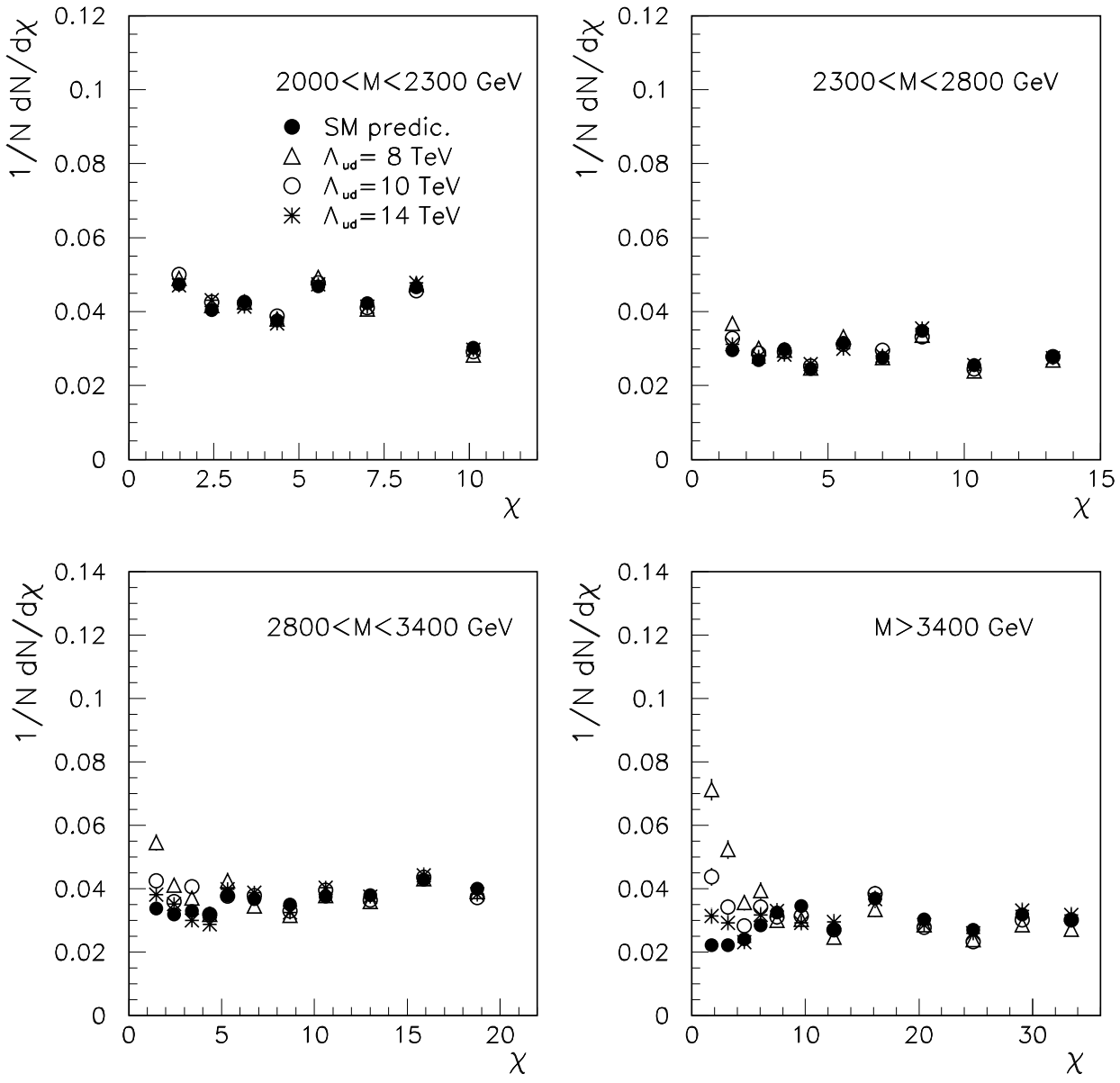

Figure 18: Compositeness in 1 fb^{-1} of ATLAS data for the two-jet angular distributions. Only up and down quarks are assumed to be composite. The Standard Model predicts fewer jets at low χ that the compositeness models [18].

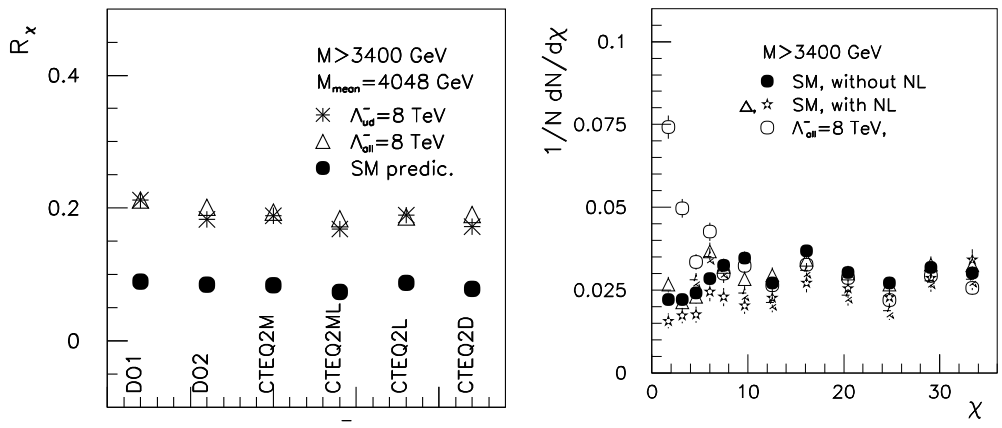

(a) (b)

Figure 19: Effect of (a) different parton distribution functions and (b) non-linearity in the jet energy scale corresponding to b = 0.11 (as in figure 17 (b)) on the two-jet angular spectrum of 1 fb^{-1} of ATLAS data [18].

the two-jet mass of the two leading jets is:

$$M = \sqrt{2E_{\perp}^{1}E_{\perp}^{2}\left(\cosh\Delta\eta - \cos\Delta\phi\right)}$$

where $E_{\perp}^{1}$ and $E_{\perp}^{2}$ are the transverse energies of the two leading jets, and $\Delta\eta$ and $\Delta\phi$ are the distance between the two jets in the pseudorapidity and azimuthal angle. This means the jet energy scale is the main source of detector related error. The resolution in η and ϕ is expected to have a small effect. In the two-jet mass analysis done by DØ [23] the resolution on the jet energy scale, η and ϕ were combined in one mass resolution function. The effect of the combined error was then estimated by modelling the two-jet mass spectrum with some function $F(M)$. That function was smeared by convoluting it with a parametrization of the mass resolution $\rho(M)$. The resulting function $f(M) = \int_0^\infty F(x)\rho(M-x)dx$ is fit to the data and used to estimate the effect of the mass resolution on the two-jet mass spectrum.

The theoretical uncertainty due to the uncertainty in the parton distribution functions is estimated by fitting the data with simulations using the CTEQ3, CTEQ4 and MRS(A) models of the PDF. The uncertainty in the simulation of the jet fragmentation was estimated by varying the renormalization and fragmentation scale from $\mu = 0.25E_{\perp}^{\max}$ to $\mu = 2E_{\perp}^{\max}$ where $E_{\perp}^{\max}$ is the highest measured jet transverse momentum.

With this method DØ has ruled out compositeness in models with constructive or destructive term in the Lagrangian at a scale of $\Lambda \leq 2.7$ GeV and $\Lambda \leq 2.4$ GeV respectively (with 95% certainty). The measurement of the two-jet mass spectrum at CDF confirms the Standard Model prediction, with slightly high values at large two-jet masses [24]. The data from CDF is in good agreement with the DØ measurement.

Note that if leptons and quarks are composite and share constituents, the mass spectrum of two-lepton events would be similarly affected. Investigating leptons avoids the non-linearity in the jet energy scale. Drell-Yan production of lepton pairs is a strong background for this compositeness measurement.

3.5 Activity During Early Running

The first ATLAS full dress rehearsal (FDR-1) took place February 4 to 8, 2008. The computing chain responsible for the reconstruction of real ATLAS data was tested with simulated samples. The performance of ATLAS detector components and reconstruction software was monitored on shifts similar to data taking shifts. Having participated in the monitoring of the liquid argon component of ATLAS and the jet reconstruction I am looking forward to participating in these shifts once ATLAS starts taking data.

Parts of the liquid argon calorimeter were designed and built at TRIUMF and the University of Victoria. So I wish to participate in the operation and monitoring of the calorimeter performance when the LHC starts running.

3.6 Summary And Outlook

The inclusive jet cross-section, two-jet angular spectrum and two-jet mass have great promise to reveal structure within the fundamental particles of the Standard Model, given enough data. If ATLAS does not collect data in a timely fashion for the completion of my thesis the inclusive jet cross-section and jet angular spectrum are still an essential test of the Standard Model. I wish to pursue my investigation of jet physics, in particular the performance of jet calibration in view of a compositeness measurement.

References

[1] J. Pumplin et al. New generation of parton distributions with uncertainties from global QCD analysis. *JHEP*, 07:012, 2002.

[2] Anthony Allen Affolder et al. Measurement of the strong coupling constant from inclusive jet production at the Tevatron $\bar{p}p$ collider. *Phys. Rev. Lett.*, 88:042001, 2002.

[3] M. R. Whalley, D. Bourilkov, and R. C. Group. The Les Houches accord PDFs (LHAPDF) and LHAGLUE. 2005. http://hepforge.cedar.ac.uk/lhapdf/.

[4] C. Grupen, Armin Böhrer, and L. Smolík. Particle detectors. *Camb. Monogr. Part. Phys. Nucl. Phys. Cosmol.*, 5:1–455, 1996.

[5] Frank Page and Sanjay Padhi. Rome jet calibration based on athena 9.0.4. March 2005.

[6] Roberto Bonciani, Stefano Catani, Michelangelo L. Mangano, and Paolo Nason. NLL resummation of the heavy-quark hadroproduction cross- section. *Nucl. Phys.*, B529:424–450, 1998.

[7] Particle Data Group. *Nuclear and Particle Physics*, pages 31–94. Institute of Physics Publishing, 2006.

[8] Stan Bentvelsen, Alexander Doxiadis, Martijn Gosselink, Manuel Kayl, Wouter Verkerke, and Ivo van Vulpen. Top-pair commissioning analysis. Top Working Group Meeting, November 7 2007.

[9] W. Verkerke and I. van Vulpen. Commissioning atlas using top-quark pair production. Atlas notes, CERN, 2007.

[10] E. Cogneras, D. Pallin, and S. Binet. Light jet energy scale determination with top events. ATLAS Physics workshop (Rome), June 2005.

[11] T.M. Liss and A. Quadt. *Review of particle physics*, volume G33, chapter The Top Quark. 2006.

[12] Gastón Leonardo Romeo, Ariel Schwartzman, and Ricardo Piegaia. Jet energy resolution using di-jet balance and kt techniques. Jet–EtMiss Phone Conference, October 2007.

[13] J. Abdallah *et al.* Atlas missing et overall performance. CSC note to be published as ATLAS internal note.

[14] F. James and M. Roos. Minuit: A System for Function Minimization and Analysis of the Parameter Errors and Correlations. *Comput. Phys. Commun.*, 10:343–367, 1975.

[15] Tom LeCompte. Standard model jet x–section. ATLAS wiki StandardModelJetXsection.

[16] H. Geiger and E. Marsden. On a diffuse reflection of the α-particles. *Proceedings of the Royal Society of London. Series A*, 82:495–500, July 1909.

[17] Vernon D. Barger and R. J. N. Phillips. *Collider Physics*. Frontiers in Physics. Addison Wesley, updated edition, December 1996.

[18] ATLAS Collaboration. Atlas detector and physics performance. Technical design report, CERN/LHCC 99-14, May 1999.

[19] A. D. Martin, W. J. Stirling, R. S. Thorne, and G. Watt. Update of Parton Distributions at NNLO. *Phys. Lett.*, B652:292–299, 2007.

[20] B. Abbott et al. Inclusive jet production in $p\bar{p}$ collisions. *Phys. Rev. Lett.*, 86:1707–1712, 2001.

[21] F. Abe et al. Measurement of dijet angular distributions at CDF. *Phys. Rev. Lett.*, 77:5336–5341, 1996.

[22] B. Abbott, M. Abolins, B. S. Acharya, I. Adam, D. L. Adams, M. Adams, S. Ahn, H. Aihara, G. A. Alves, E. Amidi, N. Amos, E. W. Anderson, R. Astur, M. M. Baarmand, A. Baden, V. Balamurali, J. Balderston, B. Baldin, S. Banerjee, J. Bantly, J. F. Bartlett, K. Bazizi, A. Belyaev, S. B. Beri, I. Bertram, V. A. Bezzubov, and P. C. Bhat. Measurement of dijet angular distributions and search for quark compositeness. *Phys. Rev. Lett.*, 80(4):666–671, Jan 1998.

[23] B. Abbott et al. The dijet mass spectrum and a search for quark compositeness in $\bar{p}p$ collisions at $\sqrt{s} = 1.8$ TeV. *Phys. Rev. Lett.*, 82:2457–2462, 1999.

[24] Anthony Allen Affolder et al. A measurement of the differential dijet mass cross section in $p\bar{p}$ collisions at $\sqrt{s} = 1.8$ TeV. *Phys. Rev.*, D61:091101, 2000.

[25] Gerald C. Blazey et al. Run II jet physics. 2000.

A Clustering

The calorimeter signal from a shower like the one displayed in figure 4 must first be separated into it's hadronic and electromagnetic components. The shower will deposit signal into a region of the calorimeter, that is a cluster of neighbouring cells. To find these clusters the calorimeter is scanned for cells with a significant signal. All cells will suffer from some electronic noise as well as background signal from pile-up. If a cell signal is stronger than four times the combined noise it is used as a seed for the clustering algorithm. For each seed all neighbouring cells with at a signal twice as strong as the combined noise for that cell are added to the cluster. Afterwards all cells along the perimeter are added iteratively if the signal from the cell is twice the background. When the iterative process finished all cells along the perimeter are added to the cluster. Clusters with common neighbours are merged. Finally clusters are split around local maxima. This algorithm is called a S=4, N=2 and P=0 algorithm to identify the threshold on cells used as seeds, neighbours and perimeter. Clusters used by other reconstruction algorithms will use values of S, N and P optimized for their purposes. Clusters are then identified as EM or hadronic by their energy density and depth within the calorimeter. This provides good separation because EM showers tend to have high energy density and are located near to the front of the calorimeter.

B Jet Algorithms

Two main issues that must be addressed for a jet algorithm to be robust are displayed in figures 20 and 21. Aside from those the algorithm should be well defined, invariant under boosts, independent

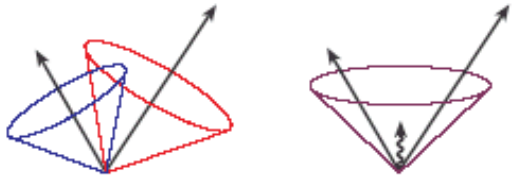

Figure 20: Illustration of sensitivity to low energy radiation in the event. A soft gluon between two jets that would have been reconstructed as two separate jets may cause the two jets to be merged into one [25].

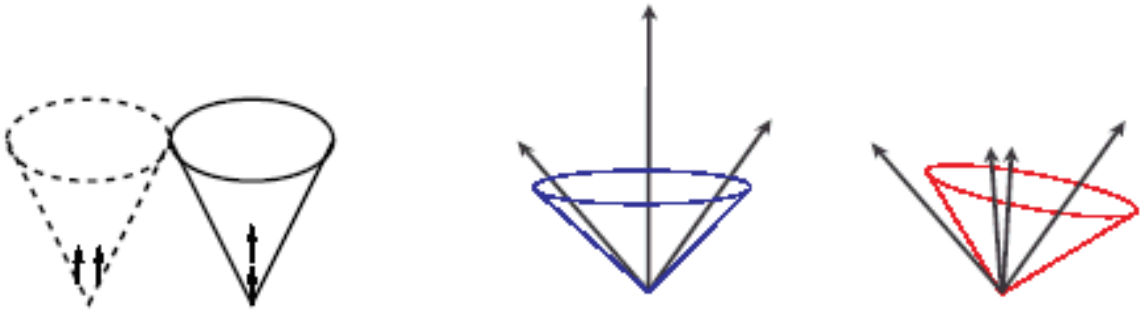

(a) (b)

Figure 21: Illustration of two problems with collinear radiation: (a) two soft collinear particles reconstructed in different towers (or clusters) may not produce a signal strong enough to seed a jet algorithm, while both particles hitting the same tower (or cluster) will seed a jet; (b) if the jet reconstruction is ordered in momentum and the energy deposited in one tower is deposited in multiple towers (or clusters) instead the jet may be reconstructed in a different place than it should [25].

of detector geometry and should run on any collection of 4-vectors. The Cone and $k_\perp$ algorithms as well as the optimal jet finder will be summarized here. In the summary the input collection of 4-vectors will be referred to as clusters though they could be any calorimeter object, tracks or even particles from the simulation.

The simplest cone algorithm creates a cone of a given $\Delta\mathcal{R}$ around every cluster. Then the energy weighted centre $\bar{C}^k = (\bar{\eta}^{C^k}, \bar{\phi}^{C^k})$ of the cone is calculated:

$$\begin{aligned} \bar{\eta}^{C^k} &= \left(\sum_{i\in C^k} E^i_\perp \eta^i\right) \cdot E_\perp^{C^k\,-1} \\ \bar{\phi}^{C^k} &= \left(\sum_{i\in C^k} E^i_\perp \phi^i\right) \cdot E_\perp^{C^k\,-1} \end{aligned} \tag{12}$$

where C^k denotes the k^{th} cone, $E_\perp^i$, η^i and ϕ^i are the transverse energy, pseudorapidity and azimuthal angle of the i^{th} cluster and $E_\perp^{C^k}$ is the total energy in the k^{th} cone. If the energy weighted centre of the cone lies outside the cluster the tower was seeded on it is erased for future iterations. All remaining cones are moved to the new energy weighted centre, a new energy weighted centre is calculated and so on allowing the cones to flow toward some local maximum of energy. The procedure is stopped when the cone centre moves less than some minimum distance. Placing a cone on every cluster in the detector makes the jet reconstruction too slow. To speed up the reconstruction only clusters above some threshold of energy are used as seeds for the cone algorithm to start with. This introduces the problems of infrared and collinear safety to make the jet reconstruction computationally feasible. A highly optimized seedless cone algorithm will be implemented in ATLAS reconstruction soon.

The $k_\perp$ algorithm writes a matrix of all clusters pairs:

$$d_{ij} = \begin{cases} {p_\perp}_{,i}^2 & \text{if } i = j \\ \min({p_\perp}_{,i}^2, {p_\perp}_{,j}^2)\frac{\Delta\mathcal{R}_{ij}^2}{D^2} & \text{if } i \neq j \end{cases} \tag{13}$$

Where ${p_\perp}_{,i}^2$ is the transverse momentum of the i^{th} cluster, D is a parameter for the algorithm[15]. d_{ij} is the minimal transverse momentum squared ($k_\perp^2$) of one cluster with respect to the other. The minimum of all d_{ij} is labelled $d_{\min}$. If $d_{\min}$ is a cluster with $i \neq j$, clusters i and j are removed from the collection of clusters and a new cluster with $E = E_i + E_j$ and $\vec{p} = \vec{p}_i + \vec{p}_j$ is added to the collection. If $d_{\min}$ is from an element with $i = j$, it is removed from the algorithm and put into the final jet collection. The process is repeated until all clusters have been moved into the jet collection.

Another recombination algorithm similar to the $k_\perp$ algorithm is the optimal jet finder (OJF) implemented for ATLAS at the University of Victoria. Instead of associating two objects as the $k_\perp$ algorithm does, the n clusters in the event are mapped to m jets:

$$p_j = \sum_{i=1}^{n} z_{ij} p_i \tag{14}$$

[15] Usually $D = 0.4$ or 0.6 at ATLAS.

where p_j are the jet 4-vectors, p_i are the cluster 4-vectors and z_{ij} is the $n \times m$ recombination matrix assigning clusters to jets. Any fraction of a cluster's momentum may be given to a jet ($0 \leq z_{ij} \leq 1$). Some fraction of a clusters energy may be assigned to soft energy rather than a jet $\bar{z}_i = 1 - \sum_{j=1}^{m} z_{ij} \leq 0$. The recombination matrix z_{ij} is determined by minimizing:

$$\Omega[\mathbf{P}, \mathbf{Q}] \cdot E_{\perp}^{\text{tot}} = \frac{Y[\mathbf{P}, \mathbf{Q}]}{R^2} + E_{\text{soft}}[\mathbf{P}, \mathbf{Q}] \tag{15}$$

where $E_{\perp}^{\text{tot}} = \sum_{i=1}^{n} E_{\perp i}$ is the scalar sum of the transverse energy of all clusters, R is a free parameter, $Y[\mathbf{P}, \mathbf{Q}] = \sum_{j=1}^{m} 2 p_j \tilde{q}_j$ is the thrust of each jet along the jet axis, $\tilde{q}_j = (1, \vec{p}_j/|\vec{p}_j|)$ is a massless 4-vector in the direction of the jet and $E_{\text{soft}}[\mathbf{P}, \mathbf{Q}] = \sum_{i=1}^{n} \bar{z}_i E_i$ is the soft radiation in the event, not associated to any jet. To find the jet configuration for an event, $\Omega[\mathbf{P}, \mathbf{Q}]$ is minimized for a minimum number of jets (m) that satisfies $\Omega[\mathbf{P}, \mathbf{Q}] < \omega_{\text{cut}}$. The OJF has two parameters (R and ω_{cut}) that may be chosen to optimize the jet finder's performance for the ATLAS environment.